Supplementary Information for

Robust Decadal Variations in ENSO Diversity, and its Impact on Future Scenarios

By Dieppois et al.

Bastien Dieppois[1, 2]*, Antonietta Capotondi[3, 4], Benjamin Pohl [5], Kwok Pan Chun[6], Paul-Arthur Monerie[7], Jonathan Eden[1]

	Institution	Name	Phase	Member	Variable	Resol. (°)	Hist. period	piC. length (yr)
Obs.	NOAA-NCDC, *USA*	ERSST.v5	o	o	sst	2	1860-2017	o
	JMA, *Japan*	COBESST.v2	o	o		1	1860-2017	o
	MOHC, UK	HadSST1	o	o		1	1860-2017	o
	NOAA, *USA*	OISST.v2	o	o	sst	0.25	1981-2017	o
	Texas A-M/NOAA-CIRES, *USA*	SODA.si3	o	8	sst	1	1860-2015	o
	NOAA-CIRES-DOE, USA	NOAA-20CR.v3	o	80	uas/vas [tau]	1	1860-2015	o
	Texas A-M/NOAA-CIRES, *USA*	SODA.v2.2.4	o	o	thetao [Z20]	0.5	1860-2008	o
CMIP5/6 Models	BCC, *China*	BCC-CSM1-1	5	3	sst	1.25	1850-2005	500
		BCC-CSM1-1-M						400
		BCC-CSM2-MR	6	3	sst	1.25	1850-2014	600
		BCC-ESM1						451
	CCCma, *Canada*	CanESM2	5	5	sst	1.25	1850-2005	996
		CanESM5	6	25	sst	1.25	1850-2014	800
	CSIRO, *Australia*	ACCESS1-0	5	1	sst	1.25	1850-2005	500
		ACCESS1-3		3				
		CSIRO-Mk3-6-0		10				
		ACCESS-ESM1-5	6	3	sst	1.25	1850-2014	900
		ACCES-CM2		2				500
	CNRM, *France*	CNRM-CM5	5	10 *(10)*	sst	1.25	1850-2005	850
		CNRM-CM6-1	6	30 *(6)*	sst, tau, Z20	1.25	1850-2014	500
		CNRM-ESM2-1		10	sst			
	INM, *Russia*	INMCM4	5	1	sst	1.25	1850-2005	500
		INMCM4-8	6	1	sst	1.25	1850-2014	530
		INMCM5-0		10				1200
	IPSL, *France*	IPSL-CM5A-LR	5	6	sst	1.25	1850-2005	1000
		IPSL-CM5A-MR		3				300
		IPSL-CM5B-LR		1				300
		IPSL-CM6A-LR	6	32 *(6)*	sst, tau, Z20	1.25	1850-2014	1200
	MIROC, *Japan*	MIROC5	5	5	sst	1.25	1850-2005	670
		MIROC6	6	10 *(10)*	sst, tau, Z20	1.25	1850-2014	800
	MOHC, *UK*	HadGEM2-CC	5	1	sst	1.25	1860-2005	240
		HadGEM2-ES		4				577
		HadGEM3-GC31-LL	6	4	sst	1.25	1850-2014	500
		HadGEM3-GC31-MM		2				500
		UKESM1-0-LL		16 *(5)*	sst, tau, Z20			1100
	KMA-MRI, *South Korea*	MRI-CGCM3	5	3	sst	1.25	1850-2005	500
		MRI-ESM2-0	6	5	sst	1.25	1860-2014	700
	MPI-M, *Germany*	MPI-ESM-LR	5	3	sst	1.25	1850-2005	1000
		MPI-ESM-MR						
		MPI-ESM1-2-HR	6	10	sst	1.25	1850-2014	500
		MPI-ESM1-2-LR						1000
	NASA-GISS, *USA*	GISS-E2-H	5	6	sst	1.25	1850-2005	780
		GISS-E2-R		6				850
		GISS-E2-R-CC		1				251
		GISS-E2-1-G	6	10	sst	1.25	1850-2014	851
		GISS-E2-1-H						401
	NCAR, *USA*	CESM1-BCG	5	1	sst	1.25	1850-2005	500
		CCSM4		6				1051
		CESM2	6	11 *(3)*	sst	1.25	1850-2014	1200
		CESM2-FV2		3				500
		CESM2-WACCM		3				499
		CESM2-WACCM-FV2		3				500
	NCC, *Norway*	NorESM1-M	5	3	sst	1.25	1850-2005	501
		NorESM1-ME		1				252
		NorCPM1	6	30	sst	1.25	1850-2014	500
		NorESM2-LM		3				391
		NorESM2-MM		1				500
	NOAA-GFDL, *USA*	GFDL-CM3	5	5	sst	1.25	1860-2005	500
		GFDL-ESM2M		1			1861-2005	
		GFDL-CM4	6	1	sst	1.25	1850-2014	500
		GFDL-ESM4		1				

Supplementary Table 1 | Summarized information on observational reference data sets, and CMIP models used in the study. Grey and orange shading delineates CMIP5 from CMIP6 models. Number of available ensemble members for future scenarios are indicated in italic.

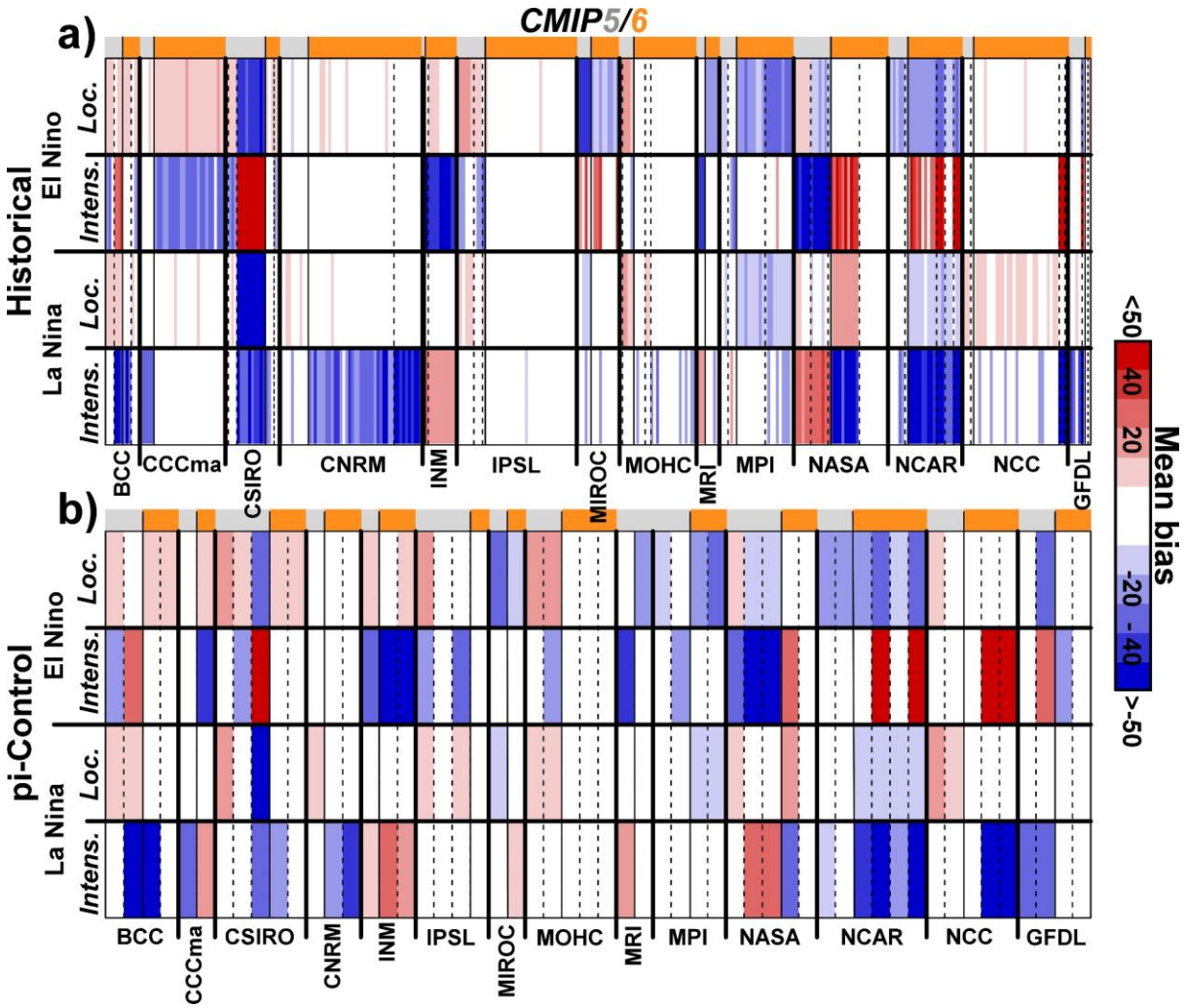

Supplementary Fig. 1 | CMIP5/6 mean bias in ENSO's location and intensity. (a) Average difference in mean location (°W) and intensity (°C) of El Niño and La Niña events between 95/250 CMIP5/6 historical runs and four long-term observational reference datasets (ERSST.v5, COBESST.v2, HadSST1, SODA.si3). **(b)** Same as **(a)** but for 26/28 CMIP5/6 piControl runs. Red (blue) shading indicates eastern/warm (western/cold) biases in ENSO location/intensity. Biases in ENSO intensity is multiplied by 100, for display purpose. Only significant differences in mean at p=0.05 using 1000 permutations in a two-sided Student's t-test are displayed.

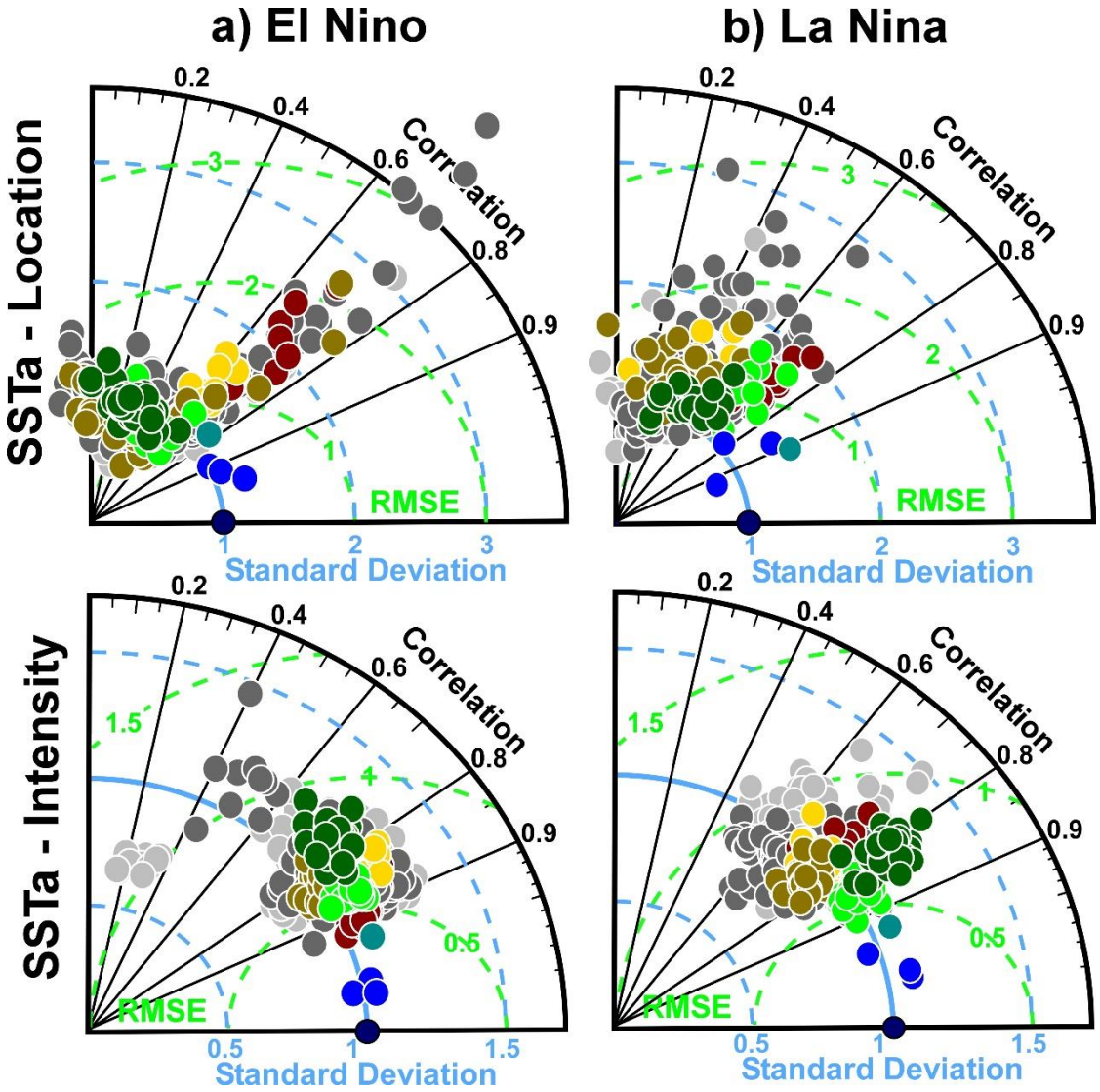

Supplementary Fig. 2 | Evaluation of model performance in simulating SSTa associated with changes in ENSO location and intensity. (a) Taylor diagrams of regressed SSTa patterns associated with changes in El Niño location (top) and intensity (bottom) from 95 CMIP5 (light grey dots) and 250 CMIP6 (dark grey dots) simulations, as compared to the observed reconstructed (blue dots) and reanalysed (sky blue dots) observational SSTa pattern. **(b)** same as **(a)** but La Niña. Models selected to study the driving mechanisms and future scenarios of ENSO diversity are highlighted in coloured dots (IPSL-CM6-LR: dark green; UKESM1-0-LL: light green; CNRM-CM5: gold; CNRM-CM6-1: yellow; MIROC6: red). The median observational changes are used as reference. The diagram is a function of the root mean square (RMSE; green dashed circles–x-axis), the correlation coefficient (black solid lines y-axis) and the standard deviation (SD; blue dashed compared to solid circles–x-axis). Since the values are normalized the reference (observation values) has a SD of 1.

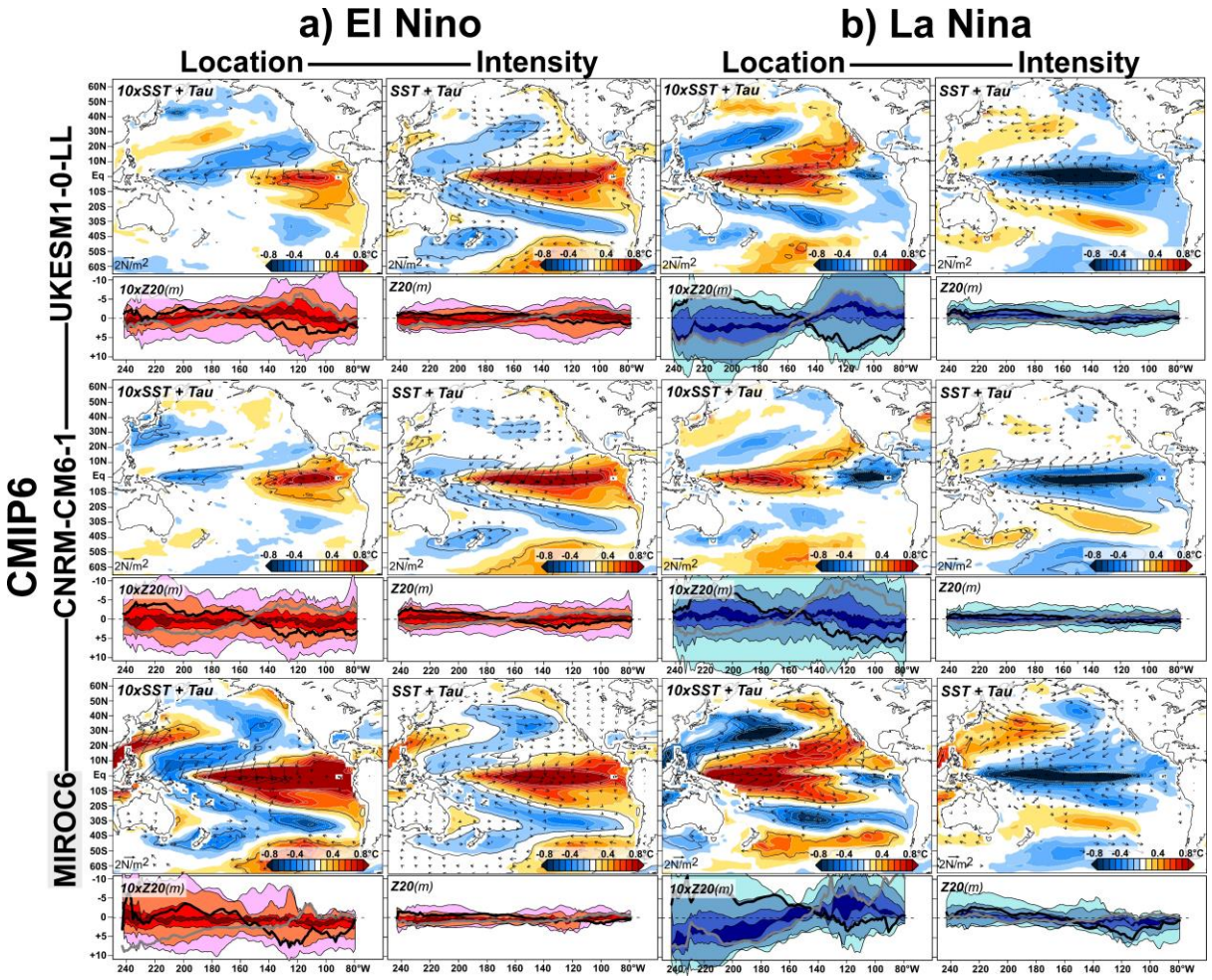

Supplementary Fig. 3 | Simulated mechanisms driving long-term variability in ENSO location and intensity in selected CMIP6 models. (a) Simulated regressed SST (blue to red shades), wind-stress (vectors) and Z20 anomalies (lines) associated with changes in El Niño location (right) and intensity (left), using UKESM1-0-LL (top), CNRM-CM6-1 (middle) and MIROC6 (bottom). **(b)** Same as **(a)** but for La Niña events. Red and blue shades on the Z20 anomalies indicate the ensemble spread (light to dark: maximum/minimum, 10/90th, 30/70th and 45/55th percentiles), for El Niño and La Niña, respectively. Group 1 (black lines) and Group 2 (grey lines) illustrate how two opposed types of equatorial Z20 anomalies influence the ensemble spread. Statistical significance is assessed at p=0.05 using 1000 permutations, and displayed as black contour for SSTa, and blue/red crosses for Z20 anomalies. Only significant wind-stress anomalies at p=0.05 are displayed.

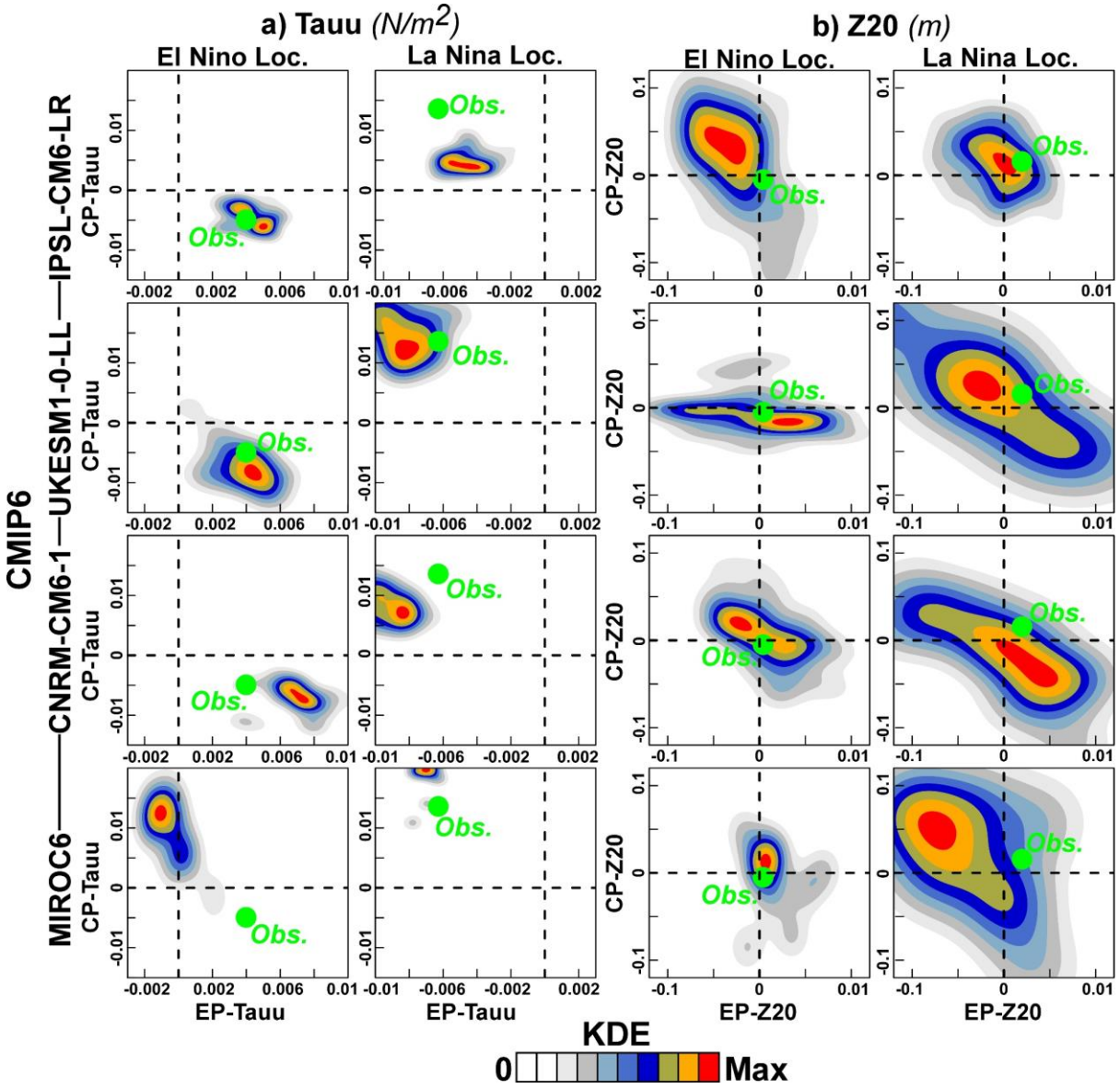

Supplementary Fig. 4 | Model performance in simulating zonal contrasts in equatorial wind-stress and Z20 in response to changes in ENSO locations. (a) Two-dimensional kernel density estimation (KDE; colour shades) of equatorial EP (x-axis) and CP (y-axis) zonal wind-stress (tauu) associated with changes in El Niño (left) and La Niña (right) location in selected CMIP6 models (top to bottom: IPSL-CM6-LR, UKESM1-0-LL, CNRM-CM6-1, MIROC6), as compared to median observed anomalies (green dot). **(b)** same as **(a)** but for differences between equatorial EP (x-axis) and CP (y-axis) thermocline depth (Z20). KDE are estimated from all ensemble members for each model. EP and CP regions here refer to 130-90°W and 221-170°W, respectively, and between 5S and 5N.

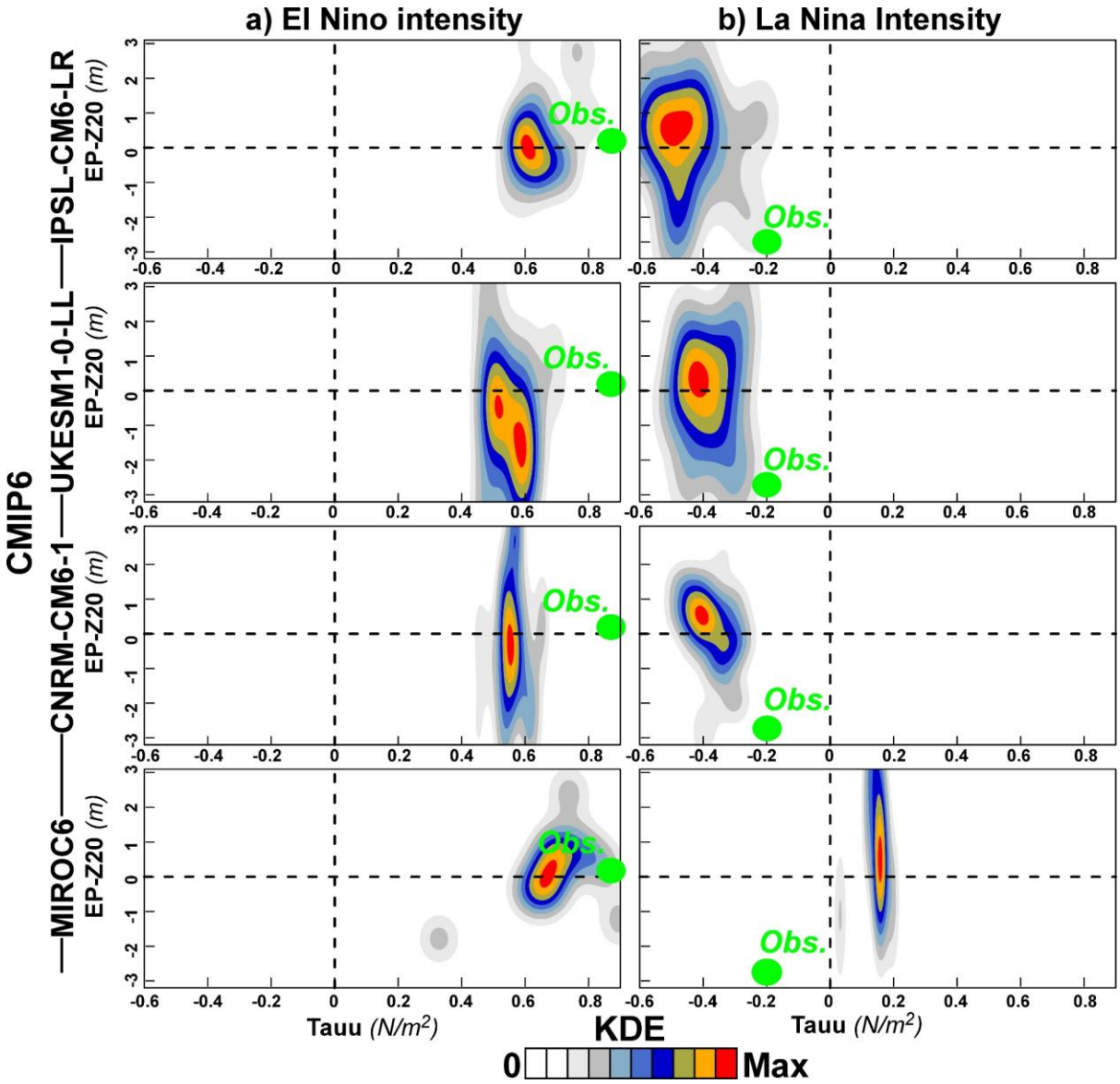

Supplementary Fig. 5 | Model performance in simulating equatorial wind-stress and and Z20 in response to changes in ENSO intensity. (a) Two-dimensional kernel density estimation (KDE; colour shades) of equatorial zonal wind-stress (tauu) and thermocline depth (Z20) associated with changes in El Niño intensity in selected CMIP6 models (top to bottom: IPSL-CM6-LR, UKESM1-0-LL, CNRM-CM6-1, MIROC6), as compared to median observed anomalies (green dot). **(b)** same as **(a)** but for La Niña intensity. KDE are estimated from all ensemble members for each model, and compared to median observed anomalies (green dot). While equatorial wind-stress are estimated between 180 and 100°W, equatorial Z20 anomalies are estimated between 130 and 90°W, but both are averaged between 5S and 5N.

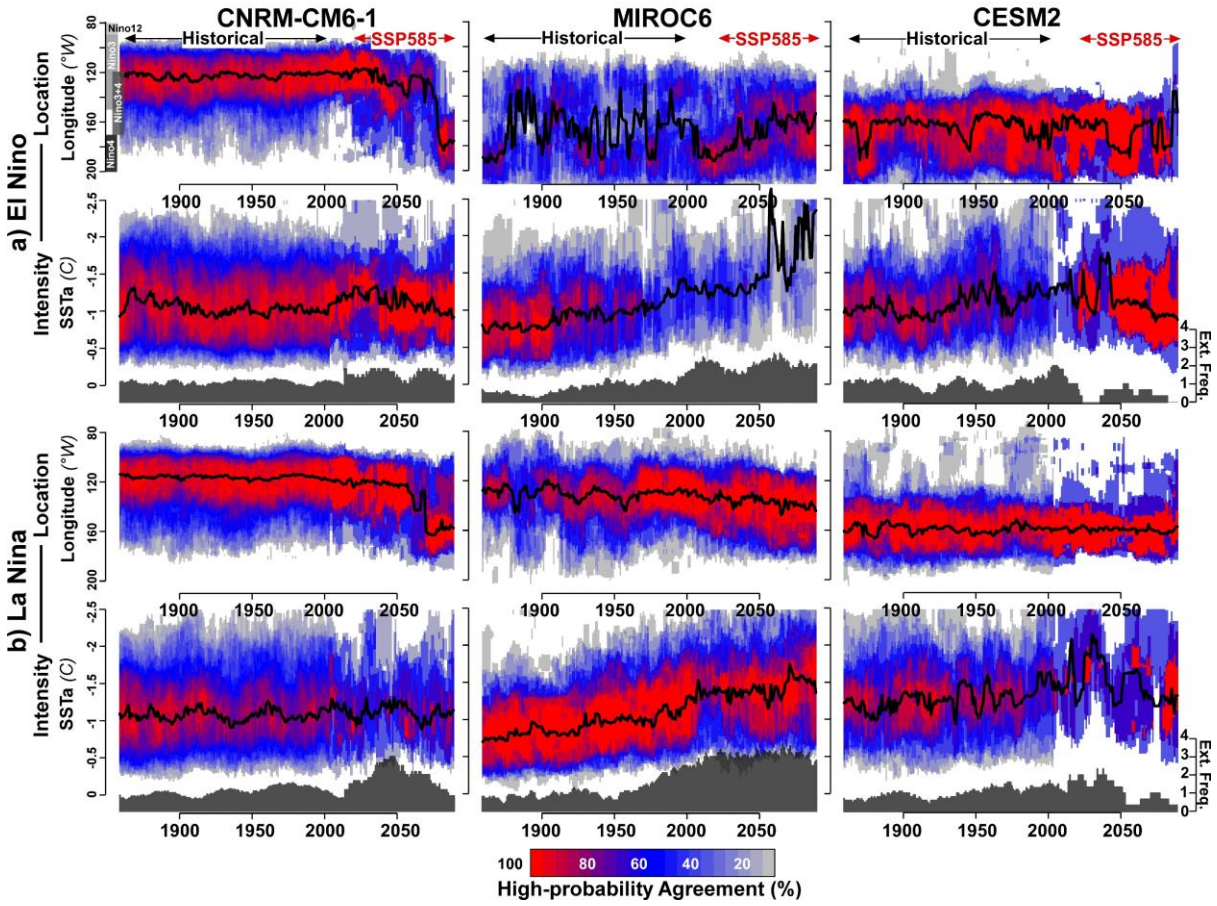

Supplementary Fig. 6 | Future scenarios for ENSO diversity in less realistic models. (a) 20-year most likely location (top) and intensity (bottom) of El Niño events (black bold lines), as well as the percentage of agreement of high-probability (*i.e.* PDF exceeding 0.01 and 0.45; colour shades) in the CNRM-CM6-1 (left), MIROC6 (middle) and CESM2 (right) model ensembles. **(b)** same as **(a)** but for La Niña events. Grey histograms on the bottom axis of the intensity panels indicate the average number of extreme events (as defined in Fig. 2) within the model ensemble. Agreement of high-probability were calculated for historical and RCP8.5/SSP5–8.5 scenarios, as the number of ensemble members differs between the two periods. Note that SSTa were estimated by removing the 1850–2014 monthly climatology and trend, to enhance comparability with observations.